Ab initio pseudopotential study of the structural and electronic properties of ZnTe under high pressure

1997 J. Phys.: Condens. Matter 9 6619

(http://iopscience.iop.org/0953-8984/9/31/014)

J. Phys.: Condens. Matter **9** (1997) 6619–6631. Printed in the UK PII: S0953-8984(97)80676-5

Ab initio pseudopotential study of the structural and electronic properties of ZnTe under high pressure

Gun-Do Lee, Chiduck Hwang, M H Lee and Jisoon Ihm

Department of Physics and Centre for Theoretical Physics, Seoul National University, Seoul 151-742, Korea

Received 6 January 1997, in final form 7 May 1997

Abstract. We have performed *ab initio* pseudopotential calculations within the local density approximation to investigate the structural phase transition of ZnTe under pressure. Zn 3d and Te 4d orbitals are treated as part of the valence states in order to describe the structural properties of ZnTe accurately. By calculating the total energy, atomic force, and stress tensors, we theoretically determine the structural phase transition of ZnTe from the zinc-blende (ZB) to the cinnabar to the distorted NaCl structure under increasing pressure. Calculational results are compared in detail with the recent experimental data obtained using angle-dispersive techniques and an image-plate detector. We also demonstrate that rotation of bonds toward lower-symmetry positions occurs at the critical pressure to relieve excessive strain. Detailed electronic structures of each phase are also presented.

1. Introduction

Most II–VI semiconductors transform from the zinc-blende (or wurtzite) structure to the NaCl structure as external pressure is applied. A known exception is that semiconductors including Hg (HgS, HgSe and HgTe) have a so-called cinnabar structure [1]. The behaviour of ZnTe under high pressure has been the focus of a variety of studies because of its unique phase diagram when compared with the other zinc chalcogenides (ZnS [2] and ZnSe [3]). An early high-pressure study on ZnTe was carried out by Samara and Drickamer [4] who found a metallic transition at around 12 GPa. In a combined x-ray diffraction and electric resistance study [5] performed later, a structural transition was found at $\sim$8.5 GPa to a nonmetallic hexagonal phase (ZnTe II) and at $\sim$13.0 GPa to a metallic phase (ZnTe III). In an x-ray absorption spectroscopy and an x-ray diffraction study [6], the values obtained for the transition pressures were 9.5 ± 0.5 and 12.0 ± 0.5 GPa. Recently, Nelmes and colleagues, equipped with angle-dispersive techniques and image-plate detectors, found rather unexpectedly that ZnTe [7] also has the cinnabar structure as well as an unusual orthorhombic structure with *Cmcm* symmetry [7] under applied pressure. This finding has created a lot of interest among both experimentalists and theorists in the structural stability of II–VI semiconductors under pressure.

We apply the *ab initio* pseudopotential plane-wave method within the local density approximation (LDA) to study the structural phase transitions of ZnTe. This method has been successfully applied to study structural phase transitions of certain semiconductors [8, 9]. However, unlike in previous calculations, there are many structural parameters to vary, and not only total energy but also atomic forces [10, 11] and stress tensors [12, 13] need to be calculated here because several competing crystal structures of ZnTe are rather complicated

0953-8984/97/316619+13$19.50

and have low-symmetry unit cells. Furthermore, to obtain good agreement with experiment, the Zn 3d and Te 4d orbitals have to be fully included in the calculation as valence electrons, which enormously increases the number of plane waves in the basis set. Pseudopotentials are generated extremely carefully so that logarithmic energy derivatives (which determine the scattering properties of the core region [14]) are accurate throughout the energy range of interest, and various convergence tests are performed to extremity (e.g., the energy cut-off (E_{cut}) is increased up to 196 Ryd). Therefore, the quality of the calculation is almost equivalent to that of an all-electron calculation, and practically the only approximation involved is the LDA.

In the next section, we will explain the computational method employed here. Section 3 will describe the calculational results and the detailed electronic and atomic structure of each phase that we have investigated. The last section summarizes important findings of the present work. Some highlights of the calculation have been reported elsewhere [15].

2. Computational method

Our calculations are performed within the LDA using the exchange–correlation potential of Ceperley and Alder [16] as parametrized by Perdew and Zunger [17]. We generate relatively soft norm-conserving pseudopotentials following the scheme of Troullier and Martins [18]. The block Davidson method [19] is used for diagonalization of large matrices, and the total energy of the system is calculated by means of the momentum-space formalism [10]. We consider the Zn 3d and Te 4d orbitals as part of the valence states. In a previous paper [20], we have shown that Zn 3d and Te 4d orbitals are essential in describing structural and electronic properties of ZnTe adequately. These pseudopotentials have been cast into the fully nonlocal separable form of Kleinman and Bylander [21] (with the s potential as the local part), and the absence of the undesired ghost states [22] has been checked. The atomic configurations used in generating the pseudopotentials are $3d^{10}4s^24p^0$ for Zn and $4d^{10}5s^25p^4$ for Te. We have used the core radii of 2.17 au for the 4s, 4p, and 3d wavefunctions of Zn, and the core radii of 1.93 au for the 5s, 5p, and 4d wavefunctions for Te. The partial core correction (PCC) [23] has been used for the Te pseudopotential to overcome the problems associated with the nonlinearity of the exchange–correlation function. We have noted that a further core correction (for Zn) does not change the result and so is unnecessary. We have tested the effect of the gradient correction (GC) to the LDA employing the method given in reference [24]. If we use both the GC and PCC, the lattice constant of the zinc-blende ZnTe is 6.2772 Å, which is larger than the experimental value (6.1037 Å) by 2.8%. If we use the GC only, the lattice constant is 6.2619 Å, still larger than the experimental value by 2.6%. Since the lattice constant and other structural properties obtained using the LDA only agree extremely well with experiment as long as the PCC is employed, we do not include the GC. (Of course, such an excellent agreement is made possible mainly by including Zn 3d and Te 4d orbitals in the calculation of valence band states, as explained in reference [20].) In the present study, eight distinct crystal structures are considered: the zinc-blende, wurtzite, CsCl, NaCl, NiAs, β-tin, cinnabar, and orthorhombic ($Cmcm$) phases. To minimize the total energy, we carry out the force and the stress calculations for each volume of the β-tin, cinnabar, or $Cmcm$ phase. (For most other structures, the force and stress calculations are unnecessary because of symmetry.) In each case, after the total energy is converged, we move individual atoms within the unit cell by an amount proportional to the forces acting on them, and recalculate the energy and the forces. We iterate this procedure until the force on each atom is smaller than 1 mRyd au^{-1}. Then we strain the primitive-lattice vectors in proportion to the stress tensor until the difference between each stress tensor component

(σ_{xx}, σ_{yy}, or σ_{zz}) and the pressure ($(\sigma_{xx}+\sigma_{yy}+\sigma_{zz})/3$) is smaller than 1% of the pressure. (For example, for the $Cmcm$ structure at 13.29 GPa, we get the stress tensor components $\sigma_{xx} = 0.904$, $\sigma_{yy} = 0.911$, and $\sigma_{zz} = 0.905$ mRyd au^{-3}.) The entire process is repeated until the energy as a function of the atomic positions and lattice vectors is converged to within 0.05 mRyd/(ZnTe basis) for the β-tin, cinnabar, and $Cmcm$ phases.

We have also tested the convergence of the basis set very carefully. Increasing the cut-off kinetic energy of the basis set (E_{cut}) to 144 Ryd gives a good convergence of the total energy (<0.1 mRyd/ZnTe) for each structure compared with the maximum E_{cut} of 196 Ryd tested in the present work. The *relative* energy among different structures is found to be stable within 0.8 mRyd/ZnTe as long as E_{cut} is above 80 Ryd. This number (0.8 mRyd) is further reduced when comparison is made between similar structures, although the absolute magnitude of the total energy converges to 10 mRyd/ZnTe. Thus, we include the plane waves up to the cut-off energy of 81 Ryd in the basis set. The typical number of plane waves is ∼5000, ∼10 000, ∼4000, ∼4000, ∼9000, ∼4000, ∼11 000, or ∼13 000 for the zinc-blende, wurtzite, CsCl, NaCl, NiAs, β-tin, cinnabar, or $Cmcm$ phase. The k-integration over the Brillouin zone is performed with the special-k-points method [25]. The number of sampling k-points in the irreducible Brillouin zone is 28, 24, 10, 28, 24, 28, 10, or 8 for the zinc-blende, wurtzite, CsCl, NiAs, NaCl, β-tin, cinnabar, or $Cmcm$ phase. (Convergence tests are carefully done for possibly confusing cases.) Since the pressure-induced phase transition of usual semiconductors, including ZnTe, is known to be insensitive to temperature (at least up to room temperature) experimentally, it is common practice to neglect the entropy contribution ($-TS$) to the Gibbs free energy and minimize the enthalpy H ($=E+PV$) to predict the transition. The pressure-induced phase transition occurs along the common tangent line of the total energy curves of the two phases, and the negative of the slope of the common tangent is the critical pressure (P_c).

3. Results and discussion

The calculated total energy curves for the eight phases have been presented in reference [15]. The zinc-blende structure is the most stable one under ambient pressure. The transition to the cinnabar phase has the smallest critical pressure (8.06 GPa) among the plausible pressure-induced phases that we study. The structure further transforms to the orthorhombic structure with the $Cmcm$ symmetry at 10.24 GPa. These results are in better agreement with experimental data (8.9 and 11.5 GPa, respectively) than other theoretical results (5.91 GPa for zinc-blende → cinnabar and 10.33 GPa for cinnabar → $Cmcm$) [26] obtained by taking the Zn 3d electrons, but not the Te 4d electrons, as part of the valence electrons. The relative error in the critical pressure (9.4% for zinc-blende → cinnabar and 11.0% for cinnabar → $Cmcm$) is a typical value in the *ab initio* LDA calculation for a quantity involving derivatives. Also note that the calculated critical pressures are for zero temperature, while the experiments were done at room temperature. The calculated P_c is actually very sensitive to a small error in energy. If the total energy curve of the cinnabar phase were to shift up by as little as 1 mRyd, the P_cs would change to 8.46 GPa (a 4.8% increase) and to 9.58 GPa (a 6.4% decrease) for the ZB → cinnabar and cinnabar → $Cmcm$ transitions respectively. If the upshift of the curve were ∼2 mRyd, the two P_cs would collapse, and the cinnabar phase would disappear. The agreement for P_c between theory and experiment with ∼10% error indicates that the accuracy of the energy difference between different crystal structures is better than 1 mRyd/atom. We believe that we have reduced all controllable errors (originating from the pseudopotential method and the incomplete convergence) to about this number, which means that the error from the LDA

is also within the same number (rather than that some accidental cancellation of different errors occurs). Since this is an upper bound for the error, the actual error in the LDA may be smaller than this; the LDA seems to give a much more accurate description of the ground-state total energy of ZnTe than is usually accepted. Now each phase is described in more detail.

3.1. ZnTe I—the zinc-blende phase

The zinc-blende structure occurs naturally as a mineral in most III–V and II–VI semiconductors. The calculation of the structural and electronic properties of ZnTe has been performed in the previous study [20], and $a_0 = 6.1026$ Å has been obtained for the lattice constant of ZnTe, in excellent agreement with the experimental value of 6.1037 Å. The calculated cohesive energy E_c is 5.76 eV, compared with the experimental value of 4.82 eV, and the calculated bulk modulus B_0 is 52.9 GPa, compared with the experimental value of 50.9 GPa. Our previous work [20] explicitly shows that there is an antibonding character in the Zn d–Te p hybridization for the Γ_{15v} state. Just before the zinc-blende phase is transformed to the cinnabar phase at 8.09 GPa, the lattice constant is 5.868 Å and the volume is reduced by 11.0% relative to the equilibrium volume.

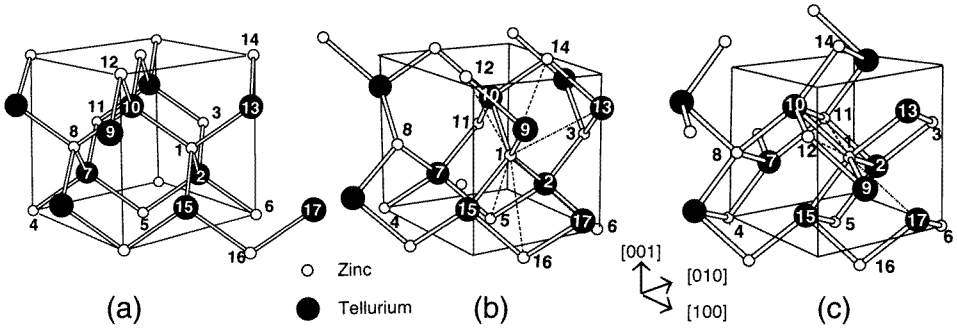

Figure 1. Atomic positions in each ZnTe structure. We draw the positions with respect to a cube to help with visualization of the structure. Note that the cube is not a unit cell for ZnTe II or ZnTe III. (a) The ZnTe I structure at 8.06 GPa (the side length of the cube = 5.868 Å); (b) the ZnTe II structure at 9.16 GPa (the side length of the cube = 5.769 Å); (c) the ZnTe III structure at 10.23 GPa (the side length of the cube = 5.718 Å). Dashed lines indicate near-neighbour bonds. The characteristic features of the atomic movement at the phase transition are described in the text.

3.2. ZnTe II—the cinnabar phase

The cinnabar structure found in HgS under ambient conditions has long been known to exist also in HgSe and HgTe under applied pressure, and regarded as a peculiarity of the mercury chalcogenides. Recently, the cinnabar structure has been found in ZnTe and CdTe as well under pressure. The cinnabar phase of ZnTe has a structure built up of infinite Zn–Te–Zn–Te spiral chains (e.g., atoms 5–2–1–10–14 in figure 1(b)), running parallel to the *c*-axis of the hexagonal unit cell. The primitive unit cell consists of six basis atoms. The cinnabar structure can be interpreted as a distorted NaCl structure. It is possible to express the structural parameters for the hypothetical cubic NaCl with respect to the unit cell of the cinnabar (hexagonal) structure. The values for *c/a*, *u*, and *v* for the cubic NaCl

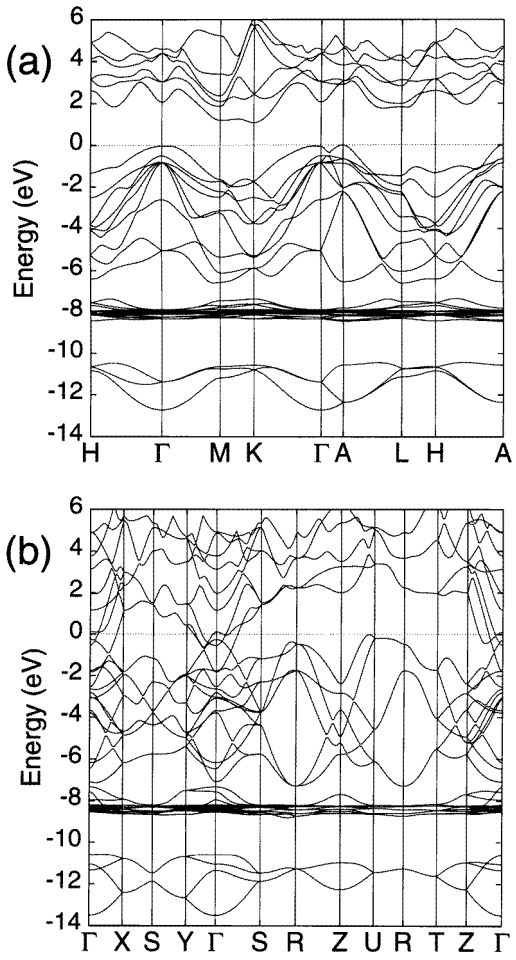

Figure 2. Calculated energy band structures of (a) ZnTe II at 9.16 GPa and (b) ZnTe III at 10.23 GPa.

would be 2.449, 0.667, and 0.667, respectively. According to the convention of reference [1], there are two a bonds (consisting of atoms 1–2 and atoms 1–9 in figure 1(b)) between nearest neighbours on the spirals, two b bonds (1–10 and 1–15) in adjacent spirals, two c bonds (1–13 and 1–17) between different atoms in adjacent spirals, and four d bonds (1–5, 1–12, 1–14, and 1–16) between the same atoms in adjacent spirals. Because the a- and b-bond lengths are nearly the same, the cinnabar structure of ZnTe is very similar to those of HgTe and CdTe which are fourfold coordinated, and different from that of HgS which is twofold coordinated. With fourfold coordination, the band structure of ZnTe II turns out to be semiconducting. It is interesting to see how various atoms move when the first-order transition occurs from ZnTe I to ZnTe II. Although there is no unique way to describe the displacement of a practically infinite number of atoms, we find that the following simplified description helps to visualize clearly the characteristic features of the structural change. In figure 1(b), in comparison with the zinc-blende structure in (a), the bond of atoms 1–2 and that of atoms 2–3 rotate clockwise with respect to the $[00\bar{1}]$ axis through atom 2 by 26° and 33° respectively. By means of this rotation, atom 1 moves away from atom 13

and approaches atom 9. An identical rotation occurs for the bonds involving the atoms 8, 7, and 11, by translational symmetry. At the calculated critical pressure (8.06 GPa), the shortest bond length in the cinnabar structure is 2.568 Å, compared with 2.541 Å for the zinc-blende structure, indicating that the strain accumulated by the applied pressure is relieved by the phase transition involving the above-mentioned rotations. Adjustments of other bonds follow to minimize the overall enthalpy. For example, if we look at the ZnTe II structure along the $[00\bar{1}]$ direction, the projected bond angles of atoms 4–7–5 and atoms 5–2–6 are 173.3° (i.e., buckled by 6.7° compared with the zinc-blende structure).

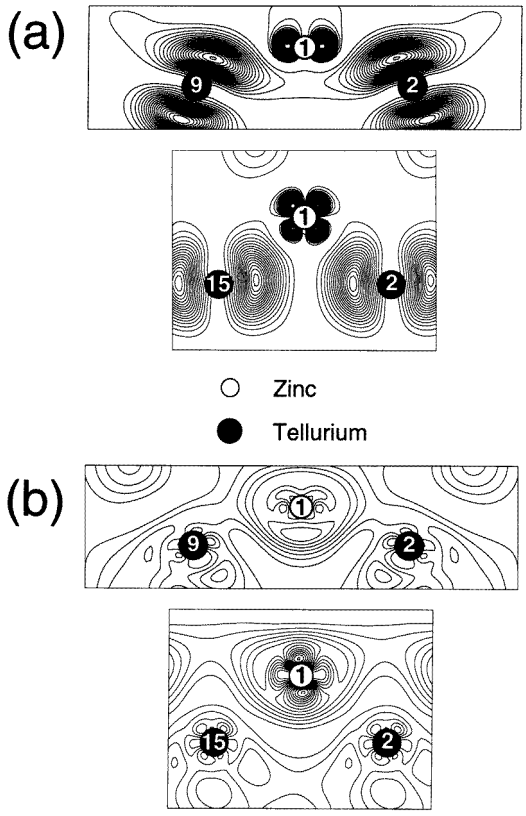

Figure 3. Contour plots of the charge density for individual states of ZnTe II on two different planes: (a) is for the VBM (at A ($k = (2\pi/c)(0, 0, 1/2)$)), (b) for the CBM (at K ($k = (2\pi/a)(1/3, \sqrt{3}/3, 0)$)), where a and c are lattice constants. The contour values run from 0.001 in steps of 0.001 electrons/unit cell. The numbers labelling the atoms are taken from those in figure 1(b).

The calculated band structure of ZnTe II is presented in figure 2(a), which shows that ZnTe II is an indirect-band-gap semiconductor with the valence band maximum (VBM) at A and the conduction band minimum (CBM) at K. The calculated band gap is 1.08 eV. (But recall that LDA substantially underestimates the gap.) The three Te s bands are placed in the energy range between −13.0 eV and −10.5 eV. There are fifteen Zn 3d bands centred at around −8.0 eV. Not shown in the figure are the fifteen Te 4d bands at around −40 eV. The finite Zn 3d-band width results from the p–d hybridization with the Te p bands. Figure 3 shows the charge-density plot of ZnTe II for the VBM state at A and the CBM state at K.

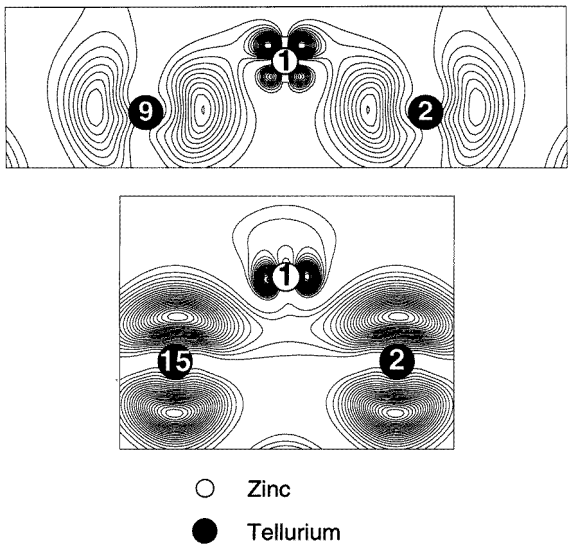

Figure 4. Contour plots of the charge density of ZnTe II for the local VBM (the Bloch eigenvalue $(E) = -0.056$ eV) at Γ on two different planes. The contour values run from 0.001 in steps of 0.001 electrons/unit cell. The numbers labelling the atoms are taken from those in figure 1(b).

For the VBM state, there are $d_{yz,zx}$ orbitals around the Zn atom. They have antibonding characters as a result of hybridization with Te ($p_{x,y}$) orbitals. Figure 4 shows the contour plot of the charge density for the state at Γ (the local maximum of the valence band). Around the Zn atom, there are d_{xy,x^2-y^2} orbitals which are hybridized with Te (p_z) orbitals and have antibonding characters. These cases are similar to those of ZnTe I [20]. The partial (i.e., site-projected, angle-decomposed) density of states (PDOS) of ZnTe II is shown in figure 5. These results involve the weighting of the total density of states by the integrated charge of a given angular momentum within the muffin-tin spheres [27]. The PDOS clearly exhibits Zn d–Te p hybridization at around -8.5 eV and near the VBM. In particular, the effects of Zn $d_{yz,zx}$ and Te p_z orbitals increase near the VBM. Near the CBM, the Zn s character is dominant, The charge-density plot (figure 3(b)) also shows that the Zn s and the Te s character prevail for the CBM state at K.

3.3. ZnTe III—the orthorhombic (Cmcm) phase

In the orthorhombic phase of ZnTe with space group *Cmcm*, the primitive unit cell consists of eight basis atoms. The cinnabar and *Cmcm* structures can each be regarded as a distorted NaCl structure, and the transition from the cinnabar to the *Cmcm* is weakly first order. In ZnTe III, alternate NaCl-like planes ($(1\bar{1}0)$ planes in figure 1(c)) are displaced approximately $+0.08$ and -0.08 along the $[11\bar{1}]$ direction, like the simple-hexagonal (SH) structure with eight contacts around each atom. However, the true SH structure has eight contacts with equal length, unlike in ZnTe III. There are one a bond (for instance, consisting of atoms 1–10 in figure 1(c)), two b bonds (1–2 and 1–9), and two c bonds (1–13 and 1–15). These five bonds have almost the same length (2.65 Å–2.73 Å). There are two d bonds of Zn–Zn contacts (1–11 and 1–12), and one e bond of a Zn–Te contact (1–17). These three bonds have almost the same length ($\approx$3.01 Å). So, the bonding arrangement in ZnTe III may be called $(5 + 3)$ coordinated. Comparing with the cinnabar structure, at critical pressure,

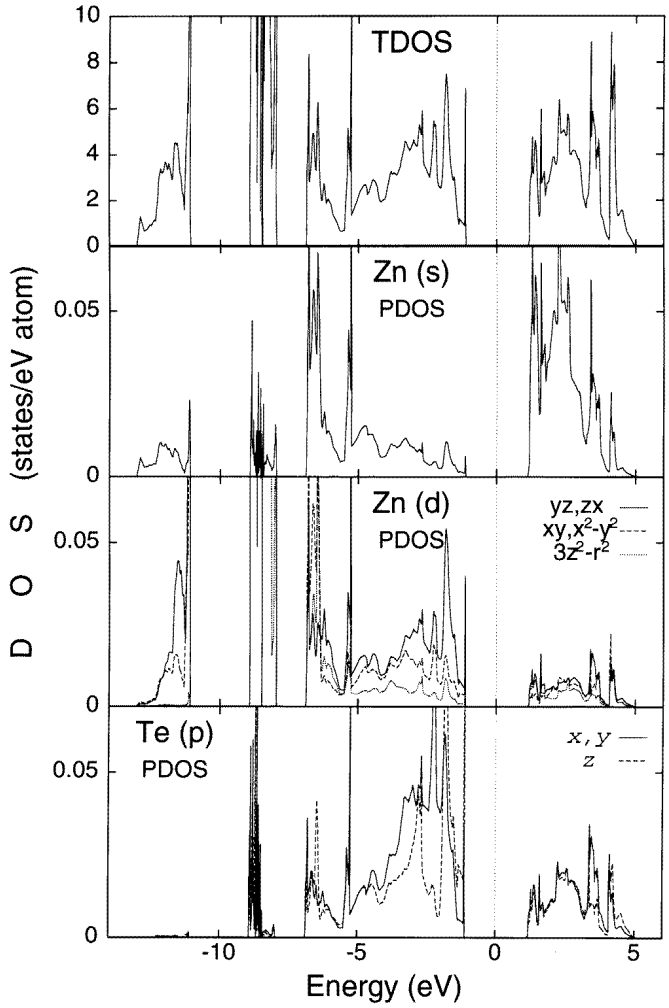

Figure 5. The TDOS and PDOS of ZnTe II. The radii of the spherical volume used to calculate the PDOS are 1.40 a_B and 1.50 a_B for Zn and Te, respectively.

the shortest bond length increases (2.553 Å $\rightarrow$ 2.655 Å). This indicates that the strain is relieved by the phase transition into a more uniform and compact structure of a higher coordination number. The band structure in figure 2(b) is metallic as expected from the high coordination number. Nelmes *et al* found that, in HgTe [28] and CdTe [29], the b bonds of the cinnabar structure increase slightly in length with increasing pressure towards the value of the nearest-neighbour distance in the NaCl structure. In addition, in their ZnTe experiment, the b-bond length (2.646 Å) of the cinnabar structure at 8.9 GPa is nearly the same as the a-bond length (2.687 Å) of the *Cmcm* structure at 15.7 GPa. According to our analysis (see figure 1) for the structural phase transition described above, the bond of atom 1–10 is the second shortest (b bond) in the cinnabar phase, and becomes the shortest one (a bond) in the *Cmcm* phase. This is consistent with the aforementioned experiments [28, 29]. As pressure increases, the *Cmcm* phase becomes more and more stable. Our calculations show that the *Cmcm* phase is stable up to very high pressure ($\gtrsim$100 GPa).

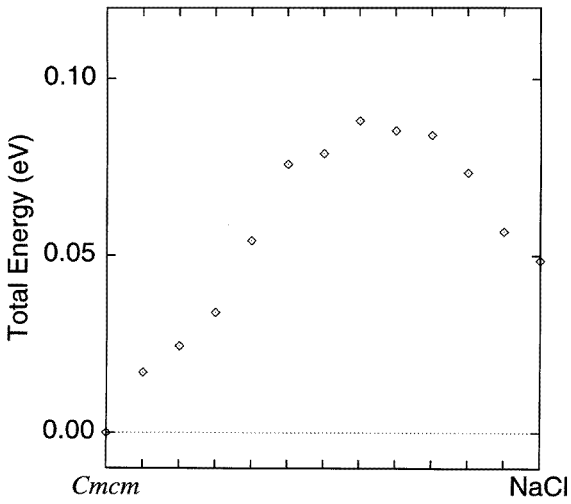

Figure 6. Total energies per ZnTe basis calculated along the path in the configuration space from the *Cmcm* structure to the NaCl structure at the volume of 980 au^3. The ordinate is the energy per ZnTe basis relative to the total energy of the optimized *Cmcm* structure.

In order to probe the energy landscape in the configuration space connecting the *Cmcm* and the NaCl structure, we calculate the total energies for each set of parameters (atomic position) which change from the *Cmcm* to the NaCl structure for a fixed volume (figure 6). All of the atomic positions are incremented by 1/12 of the total differences between those of the *Cmcm* and the NaCl structures in each step. This figure shows that the NaCl structure is a local energy minimum state for the given volume, and there exists an energy barrier of 0.1 eV per ZnTe along the path between the two structures (of course, the energy surface that we probe is an extremely small subset of the vast configuration space).

The self-consistent energy bands of ZnTe III are plotted in figure 2(b) along the symmetry directions in the irreducible Brillouin zone. There are three partially filled bands crossing E_F. One is the first band above E_F at Γ (i.e., the 59th band from the bottom at Γ), and another is the second band below E_F at Γ (i.e., the 57th band from the bottom at Γ). And still another is the fourth band below the E_F at Γ (i.e., 55th band from the bottom of at Γ). The first band below the E_F (the 58th band) is a valence band. There are four Te s bands at around -12.0 eV and twenty Zn d bands at around -8.2 eV. Not shown in the figure are the twenty Te 4d bands at around -38.3 eV. Figure 7 shows the charge density of individual states of ZnTe III near E_F. The contour plot for the 59th band at Γ (figure 7(a)) demonstrates that Zn($d_{x^2-y^2,3z^2-r^2}$) orbitals are hybridized with the Te(p_y) orbital. The contour plot of the 58th band at Γ (figure 7(b)) resembles that of the local VBM at Γ in ZnTe II (figure 4), which shows the Zn(d_{yz})$-$Te(p_z) hybridization. Figure 7(c) indicates, when compared with figure 4, that the charge density of the state is rotated according to the above-mentioned bond rotation. In the contour plot of the 57th band (figure 7(d)), we find Zn($d_{3z^2-r^2}$), Zn s, and Te s characters. According to the symmetry-decomposed partial charge analysis, the Zn s and Te s characters are the dominant characters of the state. The PDOS of ZnTe III is shown in figure 8. Near E_F, the contributions from Zn($d_{x^2-y^2,3z^2-r^2}$) and Te($p_{x,z}$) orbitals are dominant. There is also p–d hybridization at around -8.2 eV. From the PDOS analysis we see that the CBM states in the cinnabar structure and states near the Fermi level in *Cmcm* are mainly derived from Zn s states. Note that the shortest Zn–Zn

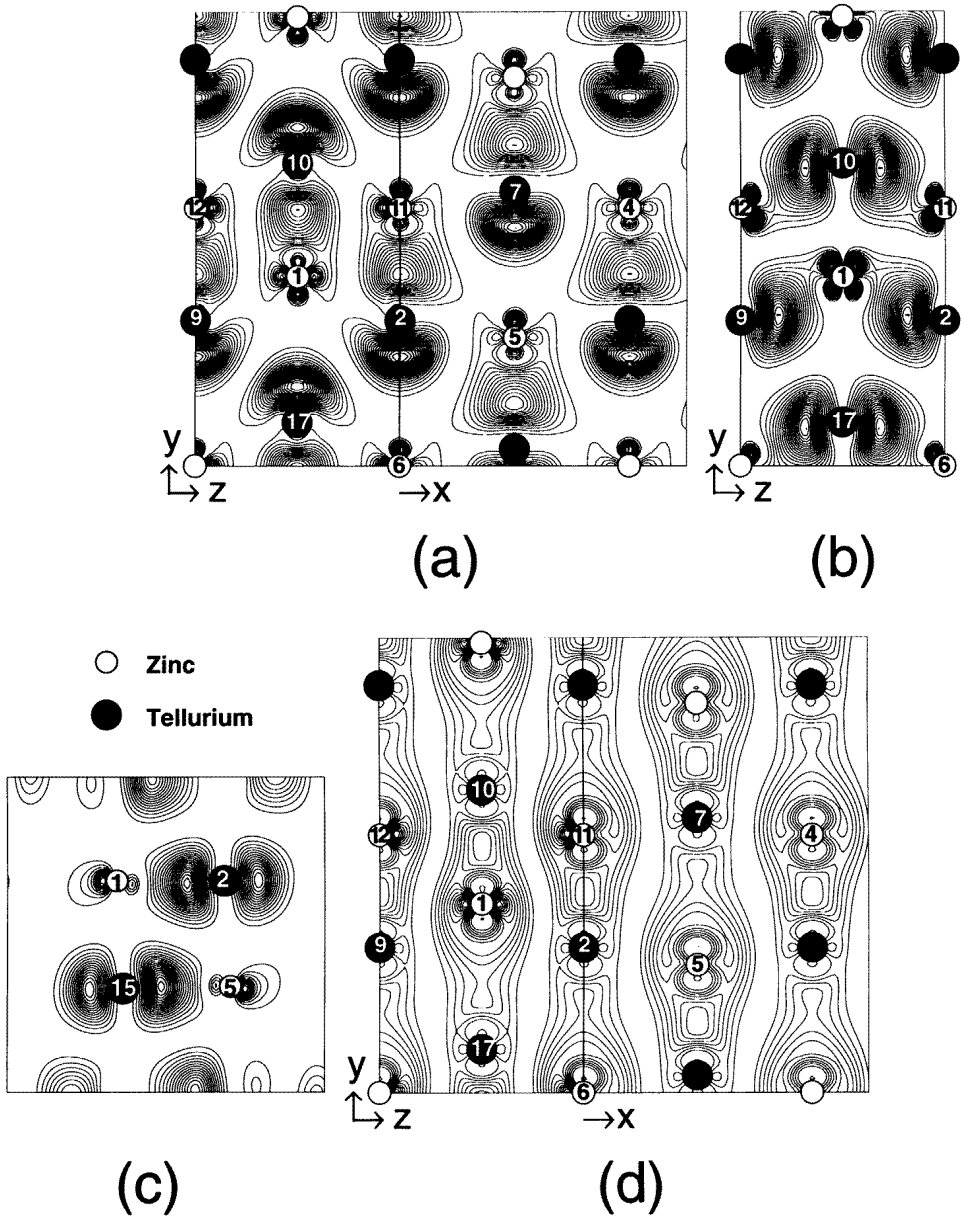

Figure 7. Contour plots of the charge density of ZnTe III for (a) the 59th band (the Bloch eigenvalue $(E) = 0.118$ eV), (b), (c) the 58th band ($E = -0.256$ eV), and (d) the 57th band ($E = -0.542$ eV) at Γ. The contour values run from 0.001 in steps of 0.001 electrons/unit cell. The numbers labelling the atoms are taken from those in figure 1(c). x, y, and z are coordinate axes for the unit cell of the *Cmcm* structure.

distances are ~3.7 Å and ~3.0 Å respectively in the cinnabar and the *Cmcm* structure. We guess that the larger overlap of Zn s orbitals due to the smaller distance induces a larger band width and the merging with the valence band, and ZnTe III becomes metallic, in contrast to ZnTe II.

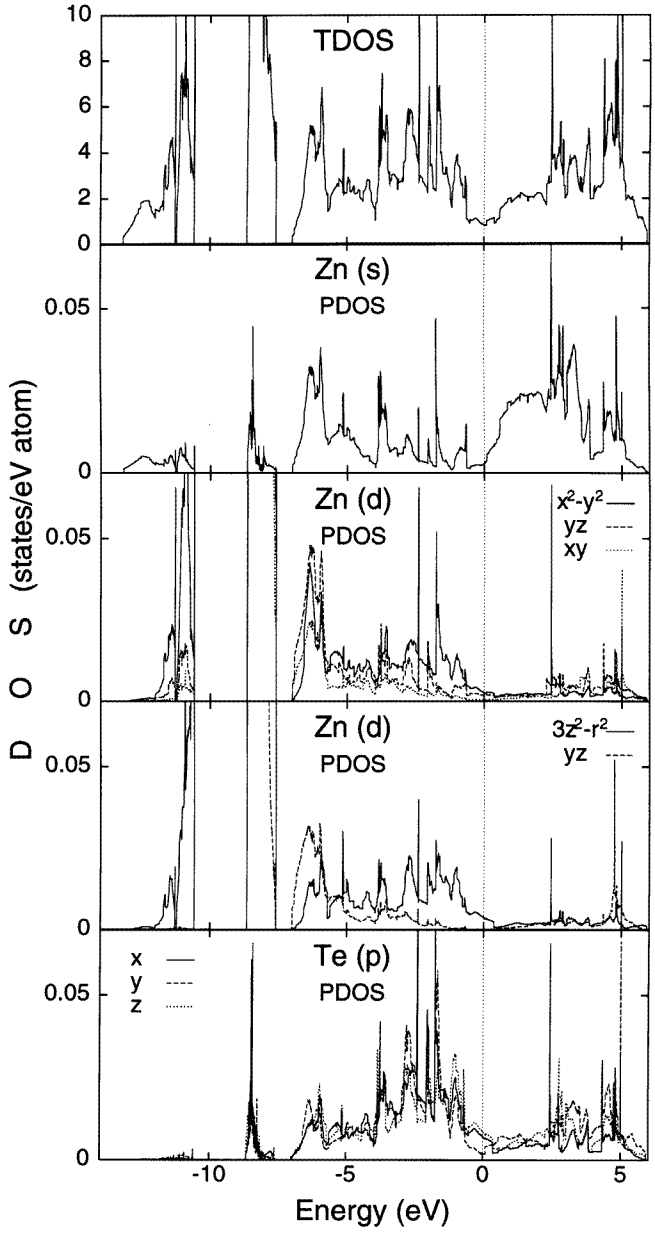

Figure 8. The TDOS and PDOS of ZnTe III. The radii of the spherical volumes used to calculate the PDOS are 1.40 a_B and 1.50 a_B for Zn and Te, respectively.

3.4. Other phases

The wurtzite, NaCl, NiAs, β-tin, and CsCl structures are not to be realized under hydrostatic pressure according to our calculation. The wurtzite structure has a hexagonal form preserving the tetrahedral bond scheme as in the zinc-blende structure. When the relative volume is below $\sim$0.7, the wurtzite structure becomes slightly lower in energy than the

Table 1. The calculated pressures and the optimized c/a ratios at each volume for the β-tin structure of ZnTe. The volumes are normalized to the equilibrium volume of the zinc-blende structure.

Volume	0.521	0.600	0.678	0.730	0.782
Pressure (GPa)	84.03	41.38	19.74	11.10	5.13
c/a	0.605	0.620	0.640	0.660	0.680

zinc-blende structure. However, the structure has already been transformed to the cinnabar to the *Cmcm* structure at such a compressed volume, and the wurtzite structure has not materialized. The NaCl structure exists in other tellurides (CdTe [30] and HgTe [28, 31]) or zinc chalcogenides (ZnS [2] and ZnSe [3]). In CdTe and HgTe, the cinnabar phase under pressure is transformed to the NaCl structure before going to the *Cmcm* structure. The NaCl structure of ZnTe has a total energy only slightly above that of the *Cmcm* structure under low pressure, but the difference becomes larger as the pressure increases. We suspect that a greater imbalance in size between the cation and the anion in ZnTe than in CdTe and HgTe favours the distorted structure over the higher-symmetry (cubic) NaCl structure. Recently, the NaCl phase of ZnTe has been reported at combined high pressure and high temperatures [32]. It is not clear whether the free energy of the NaCl structure is lowered relative to that of the *Cmcm* structure by heating. In the NiAs structure [9], the sites for the two atomic species are nonequivalent. For the ideal c/a ratio ($\sqrt{8/3}$), the anions form a hexagonal close-packed lattice, whereas the cations have a simple hexagonal structure. Each cation has the same environment as in rock-salt (NaCl) but the anion has its six neighbours hexagonally arranged. Thus the Ni–As–Ni bond angle in the plane of the c-axis is 70.5° instead of 90°. It is found that interchanging the position of the anion (Te) and the cation (Zn) further increases the total energy significantly ($\sim$0.5 eV/ZnTe). We also calculate the total energy of the β-tin phase at several different volumes. We optimize the c/a ratio by means of stress calculations for each volume. Table 1 shows the optimized c/a ratios for each volume. The β-tin structure of $c/a = 1.414(\sqrt{2})$ is equivalent to the zinc-blende structure. It is observed that, as the pressure increases, the optimized c/a ratio decreases very fast at first and then rather slowly above a few GPa, gradually approaching that of Sn or Si ($\sim$0.554). The β-tin phase that always exists in group IV semiconductors under pressure is too high in energy to be realized in ZnTe. The CsCl structure also has too high an energy to compete with the others.

4. Summary

With the use of the *ab initio* pseudopotential method, we have studied the pressure-induced structural phase transition of ZnTe. Our calculation shows that the zinc-blende phase of ZnTe is the most stable, and the structure is transformed to the cinnabar phase and again to the *Cmcm* phase as the pressure increases. Unlike the case for other tellurides and zinc chalcogenides, no NaCl phase is realized. There is no β-tin phase either, which usually exists in group IV semiconductors under high pressure. These results are in excellent agreement with experiment. We have also established that the bonds are rotated, and that the shortest bond length increases as the strain is relieved at the phase transition. Despite structural phase transitions, the Zn d–Te p antibonding character persists in each phase. Our calculated band structures show that ZnTe is an indirect-band-gap semiconductor in the cinnabar structure, and becomes metallic in the *Cmcm* phase as pressure increases. A

larger overlap of Zn s orbitals than in other structures due to a reduced Zn–Zn distance is believed to make ZnTe III metallic.

Acknowledgments

We are grateful to R J Nelmes, M I McMahon, N G Wright, and D R Allan for sending us their preprints on the high-pressure experiments on ZnTe and other semiconductors, as well as for helpful discussions. This work was supported by the Ministry of Education BSRI Programme and the Korea Science and Engineering Foundation through the SRC Programme.

References

[1] Wright N G, McMahon M I, Nelmes R J and San-Miguel A 1993 *Phys. Rev.* B **48** 13 111
[2] Smith P L and Martins J E 1965 *Phys. Lett.* **19** 541
[3] Ves S, Schwarz U, Christiansen N E, Syassen K and Cardona M 1990 *Phys. Rev.* B **42** 9113
[4] Samara G A and Drickamer H G 1962 *J. Phys. Chem. Solids* **23** 124
[5] Ohtani A, Motobayashi M and Onodera A 1980 *Phys. Lett.* **75A** 435
[6] San-Miguel A, Polian A, Gauthier M and Itié J P 1993 *Phys. Rev.* B **48** 8683
[7] Nelmes R J, McMahon M I, Wright N G and Allan D R 1994 *Phys. Rev. Lett.* **73** 1805
[8] Yin M T and Cohen M L 1982 *Phys. Rev.* B **26** 5668
[9] Froyen S and Cohen M L 1983 *Phys. Rev.* B **28** 3258
[10] Ihm J, Zunger A and Cohen M L 1979 *J. Phys. C: Solid State Phys.* **12** 4409
[11] Yin M T and Cohen M L 1982 *Phys. Rev.* B **26** 3259
[12] Nielsen O H and Martin R M 1985 *Phys. Rev.* B **32** 3792
We insert in equation (2) of this reference a missing term, $-2\sum_{\boldsymbol{G}} \boldsymbol{G}_\alpha \boldsymbol{G}_\beta V_{\mathrm{XC}}(\boldsymbol{G})\, \partial n_{\mathrm{C}}(\boldsymbol{G})/\partial(G^2)$, which takes into account the effect of the core charge. n_{C} is the core charge density inserted into the exchange–correlation potential by PCC.
[13] Bylander D M, Kleinman L and Lee S 1990 *Phys. Rev.* B **42** 1394
[14] Kerker G P 1980 *J. Phys. C: Solid State Phys.* **13** L189
[15] Lee G and Ihm J 1996 *Phys. Rev.* B **53** R7622
[16] Ceperley D M and Alder B J 1980 *Phys. Rev. Lett.* **45** 566
[17] Perdew J P and Zunger A 1981 *Phys. Rev.* B **23** 5048
[18] Troullier N and Martins J L 1991 *Phys. Rev.* B **43** 1993
[19] Davidson E R 1975 *J. Comput. Phys.* **17** 87
[20] Lee G, Lee M H and Ihm J 1995 *Phys. Rev.* B **52** 1459
[21] Kleinman L and Bylander D M 1982 *Phys. Rev. Lett.* **48** 1425
[22] Gonze X, Stumpf R and Scheffler M 1991 *Phys. Rev.* B **44** 4238
[23] Louie S G, Froyen S and Cohen M L 1982 *Phys. Rev.* B **26** 1738
[24] Ortiz G and Ballone P 1991 *Phys. Rev.* B **43** 6376
[25] Chadi D J and Cohen M L 1973 *Phys. Rev.* B **8** 5747
[26] Côté M, Zakharov O, Rubio A and Cohen M L 1997 *Phys. Rev.* B **55** 13 025
[27] Mattheiss L F and Hamann D R 1986 *Phys. Rev.* B **33** 823
[28] San-Miguel A, Wright N G, McMahon M I and Nelmes R J 1995 *Phys. Rev.* B **51** 8731
[29] McMahon M I, Nelmes R J, Wright N G and Allan D R 1993 *Phys. Rev.* B **48** 16 246
[30] Nelmes R J, McMahon M I, Wright N G and Allan D R 1995 *Phys. Rev.* B **51** 15 723
[31] Nelmes R J, McMahon M I, Wright N G and Allan D R 1995 *J. Phys. Chem. Solids* **56** 545
[32] Shimomura O, unpublished